Chiral anomaly induced nonlinear Hall effect in semimetals with multiple Weyl points

Snehasish Nandy,[1,*] Chuanchang Zeng,[2,3,*] and Sumanta Tewari[4]

[1]*Department of Physics, University of Virginia, Charlottesville, Virginia 22904, USA*

[2]*Centre for Quantum Physics, Key Laboratory of Advanced Optoelectronic Quantum Architecture and Measurement (MOE), School of Physics, Beijing Institute of Technology, Beijing 100081, China*

[3]*Beijing Key Lab of Nanophotonics & Ultrafine Optoelectronic Systems, School of Physics, Beijing Institute of Technology, Beijing 100081, China*

[4]*Department of Physics and Astronomy, Clemson University, Clemson, South Carolina 29634, USA*

(Received 20 June 2021; accepted 8 November 2021; published 22 November 2021)

After the experimental realization, the Berry curvature dipole (BCD) induced nonlinear Hall effect (NLHE) has attracted tremendous interest to the condensed matter community. Here, we investigate another family of Hall effect, namely, chiral anomaly induced nonlinear Hall effect (CNHE) in multi-Weyl semimetal (mWSM). In contrast to the BCD-induced NLHE, CNHE appears because of the combination of both chiral anomaly and anomalous velocity due to nontrivial Berry curvature. Using the semiclassical Boltzmann theory within the relaxation time approximation, we show that, in contrast to the chiral anomaly induced linear Hall effect, the magnitude of CNHE decreases with the topological charge n. Interestingly, we find that the CNHE has different behaviors in different planes for single and triple Weyl semimetals. Our prediction on the behavior of CNHE in mWSM can directly be checked in experiments.

DOI: 10.1103/PhysRevB.104.205124

I. INTRODUCTION

In recent years, the three-dimensional Dirac and Weyl semimetals have attracted tremendous interest in topological condensed matter physics. Weyl semimetals (WSMs) can accommodate gapless chiral quasiparticles, known as Weyl fermions, near the touching of a pair of nondegenerate bands (also called Weyl nodes) [1–9]. In a WSM, the nontrivial topological properties emerge due to Weyl nodes which can act as a source or sink of the Abelian Berry curvature. Each Weyl node is associated with a chirality quantum number, known as the topological charge, whose strength is related to the Chern number and is quantized in integer values [10].

Recently a number of inversion-broken and time-reversal (TR) symmetric materials such as (TaAs, $MoTe_2$, WTe_2) have been experimentally proposed as WSMs [11–15,39]. Although these systems have Weyl nodes with topological charge (n) equal to ± 1, it has been proposed that Weyl nodes with higher topological charge $n > 1$ can also be realized in condensed matter systems [9,16–18]. These are called multi-Weyl semimetals (mWSMs). Unlike the single WSM whose dispersion is linear in momentum along all directions (i.e., isotropic dispersion), the mWSM ($n > 1$) shows natural anisotropy in dispersion. In particular, the double WSM ($n = 2$) and triple WSM ($n = 3$) depict linear dispersion along one symmetry direction and quadratic and cubic energy dispersion relations for the other two directions, respectively. Using the density functional theory (DFT) calculations, it has been proposed that $HgCr_2Se_4$ and $SrSi_2$ [9,16,17] can be the candidate materials for double WSM, whereas $A(MoX)_3$ (with $A =$ Rb, TI; $X =$ Te) can accommodate triple-Weyl points [19]. It is important to note that only the Weyl nodes with topological charge $n \leqslant 3$ can be allowed in real materials due to restriction arising from discrete rotational symmetry on a lattice [16,18]. Moreover, the single WSM can be viewed as a three-dimensional (3D) analog of graphene, whereas the double WSM and triple WSM can be represented as 3D counterparts of bilayer and ABC-stacked trilayer graphene, respectively [20–22].

Weyl semimetals offer a plethora of fascinating transport properties due to the manifestation of quantum anomalies in the presence of external electromagnetic fields. Until now, chiral anomaly (also known as Adler-Bell-Jackiw anomaly) induced negative longitudinal magnetoresistance (LMR) and planar Hall effect (PHE) are the two most remarkable transport properties studied in theory and experiments [23–29]. In WSMs, the numbers of left-handed and right-handed Weyl fermions are separately conserved in the absence of any external gauge or gravitational field coupling. On the other hand, this number conservation is violated in the presence of nonorthogonal electric (**E**) and magnetic (**B**) fields (i.e., $\mathbf{E} \cdot \mathbf{B} \neq \mathbf{0}$). This effect is known as chiral anomaly [7–9,30–37]. The proposed LMR and PHE induced by the chiral anomaly have already been realized in several experiments [38–49]. The corresponding current (**J**), which is linear in electric field in both cases, can be expressed as $\mathbf{J} \propto (\mathbf{E} \cdot \mathbf{B})\mathbf{B}$.

Recently, another interesting transport property induced by chiral anomaly—nonlinear Hall effect (NLHE)—has been proposed in the context of single WSM [50]. This chiral anomaly induced nonlinear Hall effect (CNHE) is different from NLHE induced by Berry curvature dipole (BCD) [51,52]

*These authors contributed equally to this work.

because the latter can survive in the absence of external magnetic field. The CNHE is second order in electric field and appears due to the combination of both the chiral anomaly and the anomalous velocity ($\mathbf{v_a}$) due to Berry curvature ($\mathbf{\Omega_k}$). The corresponding current density can be expressed as $\mathbf{J}^{CN} = -e\sum_{\mathbf{k},s}\mathbf{v}_a^s\Delta n_{\mathbf{k}}^s$, where s is the chirality of the Weyl node, $\mathbf{v}_a^s \sim \mathbf{E}\times\mathbf{\Omega}_{\mathbf{k},s}$ [10], and $\Delta n_{\mathbf{k}}^s \sim s\mathbf{E}\cdot\mathbf{B}$ is the modification of the chiral electron density in the vicinity of each Weyl node. The NLHE caused by both the chiral anomaly as well as BCD has been studied in single WSMs [50,53–55], whereas they have not yet been explored in the context of mWSMs. Recent experimental realizations [56,57] of BCD-induced NLHE in single WSM add to the interest of experimental verification of these effects in various systems.

In this paper we investigate the chiral anomaly induced nonlinear Hall effect in mWSMs using a low-energy model. The main findings of this work are the following: Using the quasiclassical Boltzmann transport theory within the relaxation time approximation, we show that the CNHE in mWSMs can only survive in the presence of achiral tilt (i.e., tilt of the opposite chirality nodes are in the same direction) of the Weyl nodes when the Weyl nodes are at the same energy. On the other hand, this restriction no longer exists in WSMs with nonzero chiral chemical potential (i.e., the Weyl nodes are located at different energies). We further analytically show that the magnitude of CNHE depends nontrivially on topological charge n [see Eqs. (7) and (8)]. Although the dependencies are nontrivial, the magnitude of CNHE decreases with n. This is in contrast with the case of a chiral anomaly induced linear Hall effect, where the magnitude increases with n. Interestingly, the chemical potential dependence ($\mu^{-2/n}$) remains unchanged in both linear and nonlinear cases. Moreover, we also find that the CNHE shows different behavior (i.e., different coefficients) in single and triple WSMs when external electromagnetic fields are rotated in different planes, whereas they have the same behavior in the case of double WSM [see Eqs. (7) and (8)].

The rest of the paper is organized as follows. In Sec. II we formulate the general expression of CNHE using quasiclassical Boltzmann formalism. In Sec. III we introduce the low-energy Hamiltonian of multi-Weyl semimetals. In Sec. IV we derive the analytical expressions of CNHE in mWSMs and find the dependencies of CNHE with topological charge n. Finally, we summarize our results and discuss possible future directions in Sec. V.

II. FORMALISM OF CHIRAL ANOMALY INDUCED NLHE

In the presence of electric and magnetic fields, transport properties are substantially modified due to the presence of nontrivial Berry curvature, which acts as a fictitious magnetic field in the momentum space. The steady-state phenomenological Boltzmann transport equation within the relaxation time approximation takes the form [58]

$$(\dot{\mathbf{r}}\cdot\nabla_{\mathbf{r}} + \dot{\mathbf{k}}\cdot\nabla_{\mathbf{k}})g_{\mathbf{k}} = \frac{g_0 - g_{\mathbf{k}}}{\tau(\mathbf{k})}, \tag{1}$$

where $g_0 = \frac{1}{1+\exp(\epsilon_{\mathbf{k}}-\mu)/k_BT}$ is the equilibrium Fermi-Dirac distribution function, with T, μ, and $\epsilon_{\mathbf{k}}$ the temperature, chemical potential, and energy dispersion, respectively. $\tau(k)$ is the intranode scattering time, assuming the internode scattering time (τ_s) is much greater than intranode scattering time. We neglect internode scattering time because the terms related to internode scattering do not contribute to CNHE as shown in Ref. [50]. Here, $g_{\mathbf{k}}$ is the distribution function in the presence of perturbative fields. In this work we ignore the momentum dependence of τ for simplifying the calculations and assume it to be a constant [24,26,50]. In the presence of Berry curvature as well as an electromagnetic field, the semiclassical equations of motion for an electron can be written as [59,60]

$$\begin{aligned}\dot{\mathbf{r}} &= D(\mathbf{B},\mathbf{\Omega_k})\left[\mathbf{v_k} + \frac{e}{\hbar}(\mathbf{E}\times\mathbf{\Omega_k}) + \frac{e}{\hbar}(\mathbf{v_k}\cdot\mathbf{\Omega_k})\mathbf{B}\right],\\ \hbar\dot{\mathbf{k}} &= D(\mathbf{B},\mathbf{\Omega_k})\left[e\mathbf{E} + \frac{e}{\hbar}(\mathbf{v_k}\times\mathbf{B}) + \frac{e^2}{\hbar}(\mathbf{E}\cdot\mathbf{B})\mathbf{\Omega_k}\right],\end{aligned} \tag{2}$$

where $\mathbf{v_k}$ is the group velocity, and $D(\mathbf{B},\mathbf{\Omega_k}) = (1+\frac{e}{\hbar}(\mathbf{B}\cdot\mathbf{\Omega_k}))^{-1}$ is the phase-space factor as the Berry curvature $\mathbf{\Omega_k}$ modifies the phase-space volume element $dkdx \to D(\mathbf{B},\mathbf{\Omega_k})dkdx$ [59]. The term $\propto(\mathbf{E}\cdot\mathbf{B})$ is responsible for chiral anomaly which arises in axion electrodynamics of WSM. Now plugging the above equation into Eq. (1), the distribution function $g_{\mathbf{k}}$ up to second order in E for spatially uniform external fields can be obtained as $g_{\mathbf{k}} = g_0 + g_1 + g_2$, where

$$\begin{aligned}g_1 &= \frac{\tau}{D(\mathbf{B},\mathbf{\Omega_k})}\left[e\mathbf{E}\cdot\mathbf{v_k} + \frac{e^2}{\hbar}(\mathbf{E}\cdot\mathbf{B})(\mathbf{\Omega_k}\cdot\mathbf{v_k})\right]\left(\frac{\partial g_0}{\partial\epsilon_k}\right),\\ g_2 &= \frac{\tau}{D(\mathbf{B},\mathbf{\Omega_k})}\left[e\mathbf{E}\cdot\mathbf{v_k} + \frac{e^2}{\hbar}(\mathbf{E}\cdot\mathbf{B})(\mathbf{\Omega_k}\cdot\mathbf{v_k})\right]\left(\frac{\partial g_1}{\partial\epsilon_k}\right).\end{aligned} \tag{3}$$

From the general expression of the current density $\mathbf{J} = -e\int[dk]D^{-1}\dot{\mathbf{r}}g_{\mathbf{k}}$ where $[dk] = \frac{d^3k}{(2\pi)^3}$, the nonlinear Hall current density up to the order of $(\tau E^2 B)$ in the presence of external fields can be obtained as [50]

$$\begin{aligned}\mathbf{J}^{CN} = \sum_s \frac{e^4\tau}{\hbar^2}\int\frac{d^3k}{(2\pi)^3}[(\mathbf{E}\cdot\mathbf{v}_{\mathbf{k},s})(\mathbf{B}\cdot\mathbf{\Omega}_{\mathbf{k},\mathbf{s}}) - (\mathbf{E}\cdot\mathbf{B})\\ (\mathbf{v}_{\mathbf{k},s}\cdot\mathbf{\Omega}_{\mathbf{k},s})](\mathbf{E}\times\mathbf{\Omega}_{\mathbf{k},s})\left(\frac{\partial g_0^{\mathbf{k},s}}{\partial\epsilon_{\mathbf{k},s}}\right),\end{aligned} \tag{4}$$

where $\epsilon_{\mathbf{k},s}$ is the energy dispersion of a Weyl node associated with chirality s. The above equation indicates that the CNHE is a purely Fermi surface quantity and vanishes in an inversion-symmetric system. Here, we have ignored the higher-order (i.e., τ^2 dependent) contribution.

It is important to note that along with the chiral anomaly induced contribution, there may exist other contributions to the nonlinear Hall current, such as BCD-induced contribution and disorder-mediated contributions such as nonlinear side jump and skew-scattering contributions. However, the chiral anomaly induced NLHE is different from the BCD induced [52] as well as disorder-mediated NLHE [62], both of which are independent of magnetic field. Therefore, CNHE can be separated from BCD- and disorder-induced NLHE by examining their dependence on the magnetic field [52,54,55,61,62]. Moreover, the chiral anomaly induced nonlinear Hall effect

can also be differentiated from linear Hall effects by measuring second harmonic Hall resistance in ac experiments.

III. MODEL HAMILTONIAN

The low-energy effective Hamiltonian describing a Weyl node with topological charge n and chirality s can be written as [63–65]

$$H_n^s(\mathbf{k}) = s[\alpha_n k_\perp^n[\cos(n\phi_k)\sigma_x + \sin(n\phi_k)\sigma_y] + v(k_z - sQ)\sigma_z] + C_s v(k_z - sQ) - sQ_0, \quad (5)$$

where $k_\perp = \sqrt{k_x^2 + k_y^2}$, $\phi_k = \arctan(k_y/k_x)$, and σ_i's $(\sigma_x, \sigma_y, \sigma_z)$ are the Pauli matrices representing the pseudospin indices. The Weyl nodes are shifted by an amount $\pm Q$ in momentum space due to broken time-reversal symmetry, whereas the broken inversion symmetry shifts the nodes in energy by $\pm Q_0$. Here, $\alpha_n = \frac{v_\perp}{k_0^{n-1}}$, where $v_\perp$ is the effective velocity of the quasiparticles in the plane perpendicular to the z axis and k_0 represents a material-dependent parameter having the dimension of momentum. v and C_s denote the velocity and tilt parameter along the z direction, respectively. In this work, we restrict ourselves to the type-I multi-Weyl node, i.e., $|C_s| < 1$, which indicates that the Fermi surface is pointlike at the Weyl node. The energy dispersion of the multi-Weyl node associated with chirality s is given by $\epsilon_{\mathbf{k},s}^{\pm} = C_s v(k_z - sQ) - sQ_0 \pm \sqrt{\alpha_n^2 k_\perp^{2n} + v^2(k_z - sQ)^2}$, where $\pm$ represents conduction and valence bands, respectively. It is now clear that the dispersion around a Weyl node with $n = 1$ is isotropic in all momentum directions for $v = v_\perp$. On the other hand, for $n > 1$, we find that the dispersion around a double (triple) Weyl node becomes quadratic (cubic) along both k_x and k_y directions, whereas it varies linearly with k_z. Now, the different Berry curvature components of a multi-Weyl node associated with the chirality s are given by

$$\mathbf{\Omega}_{\mathbf{k},s}^{\pm} = \pm\frac{s}{2}\frac{nv\alpha_n^2 k_\perp^{2n-2}}{\beta_{\mathbf{k},s}^3}\{k_x, k_y, n(k_z - sQ)\}, \quad (6)$$

where $\beta_{\mathbf{k},s} = \sqrt{\alpha_n^2 k_\perp^{2n} + v^2(k_z - sQ)^2}$, and $\pm$ represents conduction and valence bands, respectively. It is clear from Eq. (6) that, similar to energy dispersion, the Berry curvature is isotropic in all momentum directions for the single Weyl case, whereas it becomes anisotropic for WSMs with $n > 1$, i.e., for double WSM ($n = 2$) and triple WSM ($n = 3$), due to the presence of the $k_\perp^{2n-2}$ factor and monopole charge n. The above observation itself is an indication that the multi-Weyl nature can indeed modify CNHE, which appears due to combination of both chiral anomaly and anomalous velocity induced by nontrivial Berry curvature, in double and triple WSMs as compared to the single Weyl case.

It is important to note that to calculate NLHE we assume that the Weyl nodes are reasonably well separated such that the Fermi surface is a set of disconnected regions around each Weyl node. Therefore, each Weyl node will contribute to the total CNHE additively. In a real WSM or a lattice model of a WSM where multiple pairs of Weyl node coexist, we expect that the qualitative behavior will remain similar to the linearized model studied here if we consider those Weyl nodes in the Brillouin zone whose energies are very close to the Fermi energy and add the contributions from each of those Weyl nodes.

IV. RESULTS

To calculate the different components of chiral anomaly induced nonlinear current (CNC), we apply in-plane (xy plane) electric and magnetic fields. To perform the integration [Eq. (4)] for type-I multi-Weyl semimetal, we use cylindrical coordinate geometry and make several transformations—(i) $k_\perp = k_\perp \alpha_n^{-1/n}$, $k_z = k_z/v$; (ii) $k_\perp = k_\perp^{-1/n}$; (iii) $k_\perp = k\sin\theta$, $k_z = k\cos\theta$. After some algebra, $\mathbf{J}^{CN}$ at zero temperature can be obtained as

$$[\mathbf{J}^{CN}]_{xy} = \frac{e^4\tau\alpha_n^{\frac{2}{n}}}{64\pi^{\frac{3}{2}}\hbar^2}\frac{n[n(9+2n)-2]\Gamma\left[2-\frac{1}{n}\right]}{\Gamma\left[\frac{9}{2}-\frac{1}{n}\right]} \times \sum_s \frac{C_s}{\mu_s^{2/n}}(\mathbf{E}\cdot\mathbf{B})(\hat{\mathbf{z}}\times\mathbf{E}), \quad (7)$$

where we have added the contribution of two nodes of opposite chirality. Here, $\mu_s = \mu + sQ_0$ and $\Gamma(m) = (m-1)!$ for any positive integer m. It is clear from Eq. (7) that the nonlinear current is restricted in the same plane (xy) with the applied fields and flows perpendicular to the tilt direction (z direction in current study). Therefore, we can define this effect as a *chiral anomaly induced nonlinear planar Hall effect*.

We now first consider $Q_0 = 0$, i.e., the Weyl nodes are at the same energies. In this case, it is evident from the above equation that the chiral anomaly induced nonlinear planar Hall current (CNPHC) becomes finite only when the sign of the tilt of opposite chirality nodes are the same ($C_+ = C_-$). In other words, the CNPHC vanishes in the absence of tilt ($C_+ = C_- = 0$) and even in the presence of chiral tilt ($C_+ = -C_-$) of the Weyl node. Considering $Q_0 \neq 0$, i.e., when the Weyl nodes are located in different energy, one can see from Eq. (7) that the condition for finite CNPHC changes. In this case, the CNPHC can be nonzero in both cases, i.e., for chiral as well as achiral tilt configurations of the Weyl nodes.

From Eq. (7), it is clear that the magnitude of chiral anomaly induced nonlinear Hall current depends nontrivially on topological charge n. Although the dependency is nontrivial, the magnitude of CNPHC decreases with n. This is in contrast with the case of the linear planar Hall effect where the magnitude increases with n [66]. Moreover, we also find that the multi-Weyl nature (i.e., the n dependence) also comes into CNPHC through chemical potential as $\mu_s^{-2/n}$. Interestingly, the chemical potential dependence ($\mu_s^{-2/n}$) remains unchanged in both linear and nonlinear cases [66]. These scaling factors of CNPHC with the topological charge might distinguish a single, double, and triple WSM from each other in experiment. Having done a more detailed analysis, surprisingly, we find that in the presence of nonorthogonal external fields (i.e., $\mathbf{E}\cdot\mathbf{B} \neq 0$), although the second term of Eq. (4) is contributing to CNPHC for all WSMs, the first term vanishes in the case of double WSM.

We would like to point out the most striking difference between the BCD-induced and chiral anomaly induced nonlinear Hall effect. In the case of BCD-induced nonlinear Hall

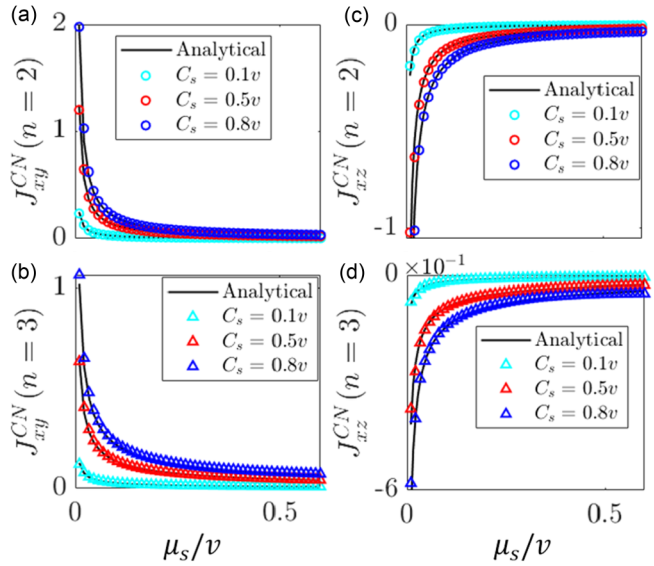

FIG. 1. Chiral anomaly induced nonlinear Hall current $\boldsymbol{J}^{CN}$ as a function of chemical potential with different tilt strengths ($C_s = 0.1, 0.5, 0.8v$) for a single multi-Weyl node with chirality $s = +1$. Panels (a, b) show the component $\boldsymbol{J}^{CN}_{xy}$ of the nonlinear Hall current with $n = 2$ and $n = 3$, respectively, while panels (c, d) show the component $\boldsymbol{J}^{CN}_{xz}$ of the nonlinear Hall current with $n = 2$ and $n = 3$, respectively. The symbols represent numerical results calculated directly from Eq. (4), while the corresponding black lines indicate the analytical results based on Eqs. (7) and (8) (for a single node $s = +1$ only). Here we use $v = 0.37$ eV Å, $v_\perp = 0.32$ eV Å, $k_0 = 0.8$ Å, $Q_0 = 0.1$ eV.

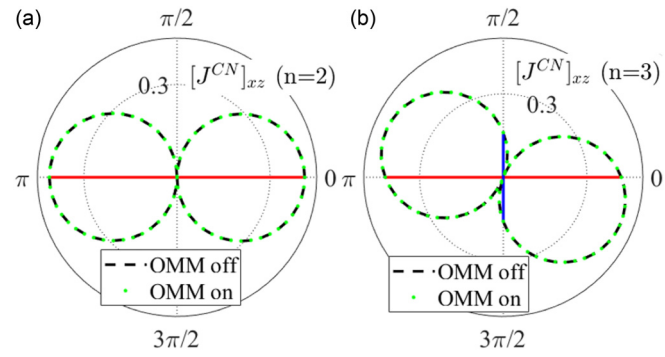

FIG. 2. The polar plot of chiral anomaly induced nonlinear Hall current $\boldsymbol{J}^{CN}_{xz}$ as a function of field angle θ (where θ is the angle between the components of electric and magnetic fields on the xz plane) for a single multi-Weyl node with chirality $s = +1$. Panels (a) and (b) show the polar distribution $\boldsymbol{J}^{CN}_{xz}(\theta)$ for $n = 2$ and $n = 3$, respectively. The solid red and blue lines indicate the magnitudes of $\boldsymbol{J}^{CN}_{xz}$ proportional to E_xB_x ($\theta = 0, \pi$) and E_zB_z ($\theta = \pi/2, 3\pi/2$), respectively. The different lengths of the blue and red lines indicate the anisotropy of the chiral anomaly induced nonlinear Hall effect in multi-Weyl systems. Note that the factor $(\hat{\boldsymbol{z}} \times \boldsymbol{E}_x)$ as given in Eq. (8) is perpendicular to the xz plane and is ignored here. We also consider the effect of orbital magnetic moment (OMM) on the magnitude of J^{CN}_{xz}; the numerical results are represented by the green dots.

effect, the contribution associated with the Weyl nodes vanishes (irrespective of the presence or absence of the tilt of the Weyl nodes). On the other hand, the whole contribution of the chiral anomaly induced nonlinear Hall effect is generated from the Weyl nodes.

Now we study the CNHE when the external fields are restricted in the xz plane. In this configuration, $\mathbf{J}^{CN}$ at zero temperature can be written as

$$[\mathbf{J}^{CN}]_{xz} = \frac{e^4\tau n\alpha_n^{\frac{2}{n}}}{64\pi^{\frac{3}{2}}\hbar^2}\left[\frac{[n(9+2n)-2]\Gamma\left[2-\frac{1}{n}\right]E_xB_x}{\Gamma\left[\frac{9}{2}-\frac{1}{n}\right]} + \frac{48n^5\Gamma\left[3-\frac{1}{n}\right]E_zB_z}{(7n-2)(5n-2)(3n-2)\Gamma\left[\frac{1}{2}-\frac{1}{n}\right]}\right] \times \sum_s \frac{C_s}{\mu_s^{2/n}}(\hat{\mathbf{z}} \times \mathbf{E}_\mathbf{x}). \quad (8)$$

The above equation suggests that unlike the xy plane, the nonlinear Hall current flows perpendicular to the plane containing external electric and magnetic fields (i.e., along y direction). Comparing Eq. (7) and Eq. (8), it is clear that in the case of $[\mathbf{J}^{CN}]_{xz}$, the coefficients proportional to $E_x^2B_x$ and $E_xE_zB_z$ are different, whereas the coefficients proportional to $E_x^2B_x$ and $E_xE_yB_y$ for J^{CN}_{xy} are the same. This leads to the fact that the current in the y direction in the presence of external electromagnetic fields restricted in the xy plane will be different when the electromagnetic fields are rotated in the xz plane. This fact gives rise to the planar anisotropy for chiral anomaly induced nonlinear Hall effect. Interestingly, we find that this planar anisotropy is present in the case of single and triple WSMs, whereas this no longer exists in double WSM.

From Eq. (8), it is clear that similar to the xy plane, the chiral anomaly induced nonlinear Hall current depends nontrivially on topological charge n. In particular, the magnitude of CNC decreases as we go from single WSM to higher-order WSMs ($n > 1$) at a fixed chemical potential. Although the topological charge dependence of CNC is different for the xz plane compared to the xy plane, the chemical potential dependence ($\mu^{-2/n}$) remains unchanged in both planes.

The analytical results obtained in Eqs. (7) and (8) agree very well with the numerical calculations, as shown in Fig. 1. Note that J^{CN}_{xy} has the same coefficients proportional to $E_x^2B_x$ and $E_xE_yB_y$, while J^{CN}_{xz} shows different coefficients proportional to $E_x^2B_x$ and $E_xE_zB_z$. To illustrate this point more clearly, we plot the magnitude of J^{CN}_{xz} as a function of angle θ, the angle formed between the projections of the electric and magnetic fields on the xz plane (i.e., $\langle \boldsymbol{E}, \boldsymbol{B} \rangle = \theta$). As shown in Fig. 2, $J^{CN}_{xz}(\theta = \pi/2, 3\pi/2)$ equals zero for the case of $n = 2$, while $J^{CN}_{xz}(n = 3)$ shows an obvious anisotropy among its x-direction [$\theta = 0, \pi/2$, the first term in Eq. (8)] and z-direction [$\theta = \pi/2, 3\pi/2$, the second term in Eq. (8)] contribution, whose magnitudes are implied by the blue and red solid lines, respectively. Interestingly, a close look into Eqs. (7) and (8) suggests that the magnitude as well as n dependence of nonlinear Hall current along the y direction is different for single and triple WSMs whereas it remains same for double WSMs.

The wave packet of a Bloch electron carries an orbital magnetic moment (OMM) in addition to its spin moment due to the self-rotation around its center of mass. The orbital moment $m(\mathbf{k})$ which couples to the magnetic field (B) through

a Zeeman-like term $\mathbf{m}(\mathbf{k})\cdot\mathbf{B}$ modifies the unperturbed band energy and quasiparticle group velocity as $\tilde{\epsilon_k} = \epsilon_k - \mathbf{m}\cdot\mathbf{B}$ and $\tilde{v_\mathbf{k}} = v_\mathbf{k} - \frac{1}{\hbar}\nabla(\mathbf{m}\cdot\mathbf{B})$ and consequently, semiclassical equations of motion. The orbital magnetic moment for a multi-Weyl node with chirality s is given by

$$\mathbf{m}^{\pm}_{\mathbf{k},s} = \frac{senv\alpha_n^2 k_\perp^{2n-2}}{2\hbar\beta^2_{\mathbf{k},s}}\{k_x, k_y, n(k_z - sQ)\}, \tag{9}$$

where $\pm$ represents valence and conduction bands, respectively. It is clear from Eq. (9) that the orbital magnetic moment is anisotropic in mWSMs compared to single WSM. In order to calculate chiral anomaly induced nonlinear Hall current numerically in mWSMs, we have chosen $k_0 = 0.8$, $v = 0.37$ eV Å, $v_\perp = 0.32$ eV Å, $|C_s| = 0.8$, $Q_0 = 0$, $Q = 0$. We find that the presence of orbital magnetic moment does not affect the magnitude of J^{CN}, as shown in Fig. 2. This feature, distinct from that in the anomalous responses in the linear regime [67–69], in turn can also be used to distinguish the chiral anomaly induced nonlinear Hall effect from linear Hall effects in experiments.

V. DISCUSSION AND CONCLUSION

We investigate the chiral anomaly induced nonlinear Hall effect in multi-Weyl semimetals. In the presence of nonorthogonal electromagnetic fields, it appears because of the combination of both chiral anomaly and anomalous velocity due to nontrivial Berry curvature in WSM. Using the quasiclassical Boltzmann theory within the relaxation time approximation, we have predicted the behavior of CNHE considering a low-energy model of type-I mWSMs, specifically, using two separate multi-Weyl nodes of opposite chiralities in the presence of external electric and magnetic fields rotating in the (i) xy plane and (ii) xz plane.

We find that the chiral anomaly induced nonlinear Hall current flows perpendicular to the tilt direction, i.e., perpendicular to the z direction in the present work. In both cases we show that when the Weyl nodes are located at the same energy, the CNHE in mWSMs can only be nonzero in the presence of achiral tilt (i.e., tilt of the opposite chirality nodes are in the same direction) of the Weyl nodes. Interestingly, this restriction no longer exists when the Weyl nodes are located at different energies in WSM (i.e., in the presence of a nonzero chiral chemical potential). We further analytically show that, in both cases, the magnitude of CNHE depends nontrivially on topological charge n [see Eqs. (7) and (8)]. Although the dependencies are nontrivial, the magnitude of CNHE decreases with n. This is in contrast with the case of chiral anomaly induced linear Hall effect where the magnitude increases with n. Interestingly, the chemical potential dependence ($\mu_s^{-2/n}$) remains unchanged in both linear and nonlinear cases.

We find that the CNHE shows different behavior (i.e., different coefficients) when external electromagnetic fields are rotated in different planes [see Eqs. (7) and (8)]. Specifically, we find that the current in the y direction with the external electromagnetic fields rotated in the xy plane will be different than the case when the external electromagnetic fields are rotated in the xz plane. This fact gives rise to the planar anisotropy for chiral anomaly induced nonlinear Hall effect. Interestingly, we find that this planar anisotropy is present in the case of single and triple WSMs, whereas this no longer exists in double WSM. Therefore, the CNHE can be used as a probe to distinguish single, double, and triple WSMs from each other in experiments. We also find that unlike the linear response case, the orbital magnetic moment has no affect on CNHE.

In contrast to the linearized model we used in this work, a real mWSM may contain Weyl nodes with different tilts with respect to one another, and a number of pair of nodes can be greater than 1. In addition, the CNHE calculated using the low-energy model becomes dependent on the momentum cutoff in the case of type-II mWSMs [50]. On the other hand, we know that a lattice model of Weyl fermions with lattice regularization provides a natural ultraviolet cutoff to the low-energy Dirac spectrum. Therefore, to predict the quantitatively correct experimental behavior of CNHE in mWSMs, one needs to study a mWSM Hamiltonian using DFT or a lattice Hamiltonian of an inversion-broken mWSM. Finding a lattice description of an inversion-broken mWSM and calculation of CNHE are interesting questions which we leave for future study. Investigating CNHE in the quantum regime (high magnetic field), where the Landau-level quantization is applicable, would also be a fascinating question to look into. Similar to a chiral anomaly induced linear Nernst effect [66,70], we also expect a finite nonlinear Nernst effect induced by chiral anomaly in mWSMs, which is yet to be explored.

ACKNOWLEDGMENTS

S.N. acknowledges National Science Foundation Grant No. DMR-1853048. C.Z. acknowledges support from the fellowship of the China Postdoctoral Science Foundation (Grant No. 2021M690409) and the National Key R&D Program of China (Grant No. 412 2020YFA0308800). S.T. thanks the NSF for support through Grant No. 2014157.

[1] S. Murakami, New J. Phys. **9**, 356 (2007).
[2] S. Murakami, S. Iso, Y. Avishai, M. Onoda, and N. Nagaosa, Phys. Rev. B **76**, 205304 (2007).
[3] M. E. Peskin and D. V. Schroeder, *An Introduction to Quantum Field Theory* (Westview Press, Boulder, CO, 1995).
[4] K. Y. Yang, Y. M. Lu, and Y. Ran, Phys. Rev. B **84**, 075129 (2011).
[5] A. A. Burkov, M. D. Hook, and L. Balents, Phys. Rev. B **84**, 235126 (2011).
[6] A. A. Burkov and L. Balents, Phys. Rev. Lett. **107**, 127205 (2011).
[7] X. Wan, A. M. Turner, A. Vishwanath, and S. Y. Savrasov, Phys. Rev. B **83**, 205101 (2011).
[8] G. Volovik and M. Zubkov, Nucl. Phys. B **881**, 514 (2014).

[9] G. Xu, H. Weng, Z. Wang, X. Dai, and Z. Fang, Phys. Rev. Lett. **107**, 186806 (2011).

[10] D. Xiao, M. C. Chang, and Q. Niu, Rev. Mod. Phys. **82**, 1959 (2010).

[11] B. Q. Lv, N. Xu, H. M. Weng, J. Z. Ma, P. Richard, X. C. Huang, L. X. Zhao, G. F. Chen, C. E. Matt, F. Bisti, V. N. Strocov, J. Mesot, Z. Fang, X. Dai, T. Qian, M. Shi, and H. Ding, Nat. Phys. **11**, 724 (2015).

[12] S-Y. Xu, I. Belopolski, N. Alidoust, M. Neupane, G. Bian, C. Zhang, R. Sankar, G. Chang, Z. Yuan, C-C. Lee, S-M. Huang, H. Zheng, J. Ma, D. S. Sanchez, B. Wang, A. Bansil, F. Chou, P. P. Shibayev, H. Lin, S. Jia, and M. Z. Hasan, Science **349**, 9297 (2015).

[13] Y. Wu, D. Mou, N. H. Jo, K. Sun, L. Huang, S. L. Bud'Ko, P. C. Canfield, and A. Kaminski, Phys. Rev. B **94**, 121113(R) (2016).

[14] J. Jiang, Z. K. Liu, Y. Sun, H. F. Yang, C. R. Rajamathi, Y. P. Qi, L. X. Yang, C. Chen, H. Peng, C. C. Hwang, S. Z. Sun, S. K. Mo, I. Vobornik, J. Fujii, S. S. P. Parkin, C. Felser, B. H. Yan, and Y. L. Chen, Nat. Commun. **8**, 13973 (2017).

[15] B. Yan and C. Felser, Annu. Rev. Condens. Matter Phys. **8**, 337 (2017).

[16] C. Fang, M. J. Gilbert, X. Dai, and B. A. Bernevig, Phys. Rev. Lett. **108**, 266802 (2012).

[17] S.-M. Huang, S.-Y. Xu, I. Belopolski, C.-C. Lee, G. Chang, T.-R. Chang, B. Wang, N. Alidoust, G. Bian, M. Neupane, D. Sanchez, H. Zheng, H.-T. Jeng, A. Bansil, T. Neupert *et al.*, Proc. Nat. Acad. Sci. USA **113**, 1180 (2016).

[18] B. J. Yang and N. Nagaosa, Nat. Commun. **5**, 4898 (2014).

[19] Q. Liu and A. Zunger, Phys. Rev. X **7**, 021019 (2017).

[20] E. McCann and V. I. Falâko, Phys. Rev. Lett. **96**, 086805 (2006).

[21] F. Guinea, A. H. Castro Neto, and N. M. R. Peres, Phys. Rev. B **73**, 245426 (2006).

[22] H. Min and A. H. MacDonald, Phys. Rev. B **77**, 155416 (2008).

[23] A. A. Burkov, J. Phys.: Condens. Matter **27**, 113201 (2015).

[24] D. T. Son and B. Z. Spivak, Phys. Rev. B **88**, 104412 (2013).

[25] V. A. Zyuzin, Phys. Rev. B **95**, 245128 (2017).

[26] K-S. Kim, H-J. Kim, and M. Sasaki, Phys. Rev. B **89**, 195137(R) (2014).

[27] S. Nandy, G. Sharma, A. Taraphder, and S. Tewari, Phys. Rev. Lett. **119**, 176804 (2017).

[28] A. A. Burkov, Phys. Rev. B **96**, 041110(R) (2017).

[29] S. Ghosh, D. Sinha, S. Nandy, and A. Taraphder, Phys. Rev. B **102**, 121105(R) (2020).

[30] P. Goswami and S. Tewari, Phys. Rev. B **88**, 245107 (2013).

[31] J. S. Bell and R. A. Jackiw, Nuovo Cimento A **60**, 47 (1969).

[32] V. Aji, Phys. Rev. B **85**, 241101(R) (2012).

[33] S. Adler, Phys. Rev. **177**, 2426 (1969).

[34] H. B. Nielsen and M. Ninomiya, Phys. Lett. B **105**, 219 (1981).

[35] H. B. Nielsen and M. Ninomiya, Phys. Lett. B **130**, 389 (1983).

[36] A. A. Zyuzin, S. Wu, and A. A. Burkov, Phys. Rev. B **85**, 165110 (2012).

[37] S. Zhong, J. Orenstein, and J. E. Moore, Phys. Rev. Lett. **115**, 117403 (2015).

[38] L. P. He, X. C. Hong, J. K. Dong, J. Pan, Z. Zhang, J. Zhang, and S. Y. Li, Phys. Rev. Lett. **113**, 246402 (2014).

[39] X. Huang, L. Zhao, Y. Long, P. Wang, D. Chen, Z. Yang, H. Liang, M. Xue, H. Weng, Z. Fang, X. Dai, and G. Chen, Phys. Rev. X **5**, 031023 (2015).

[40] T. Liang, Q. Gibson, M. N. Ali, M. Liu, R. J. Cava, and N. P. Ong, Nat. Mater. **14**, 280 (2015).

[41] C.-L. Zhang, S.-Y. Xu, I. Belopolski, Z. Yuan, Z. Lin, B. Tong, G. Bian, N. Alidoust, C.-C. Lee, S.-M. Huang, T.-R. Chang, G. Chang, C.-H. Hsu, H.-T. Jeng, M. Neupane, D. S. Sanchez, H. Zheng, J. Wang, H. Lin, C. Zhang *et al.*, Nat. Commun. **7**, 10735 (2016).

[42] Q. Li, D. E. Kharzeev, C. Zhang, Y. Huang, I. Pletikosic, A. V. Fedorov, R. D. Zhong, J. A. Schneeloch, G. D. Gu, and T. Valla, Nat. Phys. **12**, 550 (2016).

[43] J. Xiong, S. K. Kushwaha, T. Liang, J. W. Krizan, M. Hirschberger, W. Wang, R. J. Cava, and N. P. Ong, Science **350**, 413 (2015).

[44] F. C. Chen, X. Luo, J. Yan, Y. Sun, H. Y. Lv, W. J. Lu, C. Y. Xi, P. Tong, Z. G. Sheng, X. B. Zhu, W. H. Song, and Y. P. Sun, Phys. Rev. B **98**, 041114(R) (2018).

[45] M-X. Deng, H-J. Duan, W. Luo, W. Y. Deng, R-Q. Wang, and L. Sheng, Phys. Rev. B **99**, 165146 (2019).

[46] R. Singha, S. Roy, A. Pariari, B. Satpati, and P. Mandal, Phys. Rev. B **98**, 081103(R) (2018).

[47] P. Li, C. H. Zhang, J. W. Zhang, Y. Wen, and X. X. Zhang, Phys. Rev. B **98**, 121108(R) (2018).

[48] D. D. Liang, Y. J. Wang, W. L. Zhen, J. Yang, S. R. Weng, X. Yan, Y. Y. Han, W. Tong, W. K. Zhu, L. Pi, and C. J. Zhang, AIP Adv. **9**, 055015 (2019)

[49] N. Kumar, S. N. Guin, C. Felser, and C. Shekhar, Phys. Rev. B **98**, 041103(R) (2018).

[50] R.-H. Li, O. G. Heinonen, A. A. Burkov, and S. S.-L. Zhang, Phys. Rev. B **103**, 045105 (2021).

[51] T. Morimoto, S. Zhong, J. Orenstein, and J. E. Moore, Phys. Rev. B **94**, 245121 (2016).

[52] I. Sodemann and L. Fu, Phys. Rev. Lett. **115**, 216806 (2015).

[53] Y. Zhang, Y. Sun, and B. Yan, Phys. Rev. B **97**, 041101(R) (2018).

[54] O. Matsyshyn and I. Sodemann, Phys. Rev. Lett. **123**, 246602 (2019).

[55] C. Zeng, S. Nandy, and S. Tewari, Phys. Rev. B **103**, 245119 (2021).

[56] K. Kang, T. Li, E. Sohn, J. Shan, and K. F. Mak, Nat. Mater. **18**, 324 (2019).

[57] Q. Ma, S.-Y. Xu, H. Shen, D. Macneill, V. Fatemi, T.-R. Chang, A. M. Mier Valdivia, S. Wu, Z. Du, C.-H. Hsu *et al.*, Nature (London) **565**, 337 (2019).

[58] J. M. Ziman, *Electrons and Phonons: The Theory of Transport Phenomena in Solids* (Clarendon Press, Oxford, UK, 2001).

[59] C. Duval, Z. Horvth, P. A. Horvthy, L. Martina, and P. C. Stichel, Mod. Phys. Lett. B **20**, 373 (2006).

[60] D. T. Son and N. Yamamoto, Phys. Rev. Lett. **109**, 181602 (2012).

[61] E. J. Koönig, M. Dzero, A. Levchenko, and D. A. Pesin, Phys. Rev. B **99**, 155404 (2019).

[62] S. Nandy and I. Sodemann, Phys. Rev. B **100**, 195117 (2019).

[63] X. Li, B. Roy, and S. Das Sarma, Phys. Rev. B **94**, 195144 (2016).

[64] S. P. Mukherjee and J. P. Carbotte, Phys. Rev. B **97**, 045150 (2018).

[65] R. M. A. Dantas, F. Pena-Benitez, B. Roy, and P. Surowka, J. High Energy Phys. 12 (2018) 069.

[66] T. Nag and S. Nandy, J. Phys.: Condens. Matter **33**, 075504 (2020).

[67] S. Nandy, A. Taraphder, and S. Tewari, Sci. Rep. **8**, 14983 (2018).
[68] K. Das and A. Agarwal, Phys. Rev. B **100**, 085406 (2019).
[69] G. Sharma, S. Nandy, and S. Tewari, Phys. Rev. B **102**, 205107 (2020).
[70] G. Sharma, P. Goswami, and S. Tewari, Phys. Rev. B **93**, 035116 (2016).